Chemical Engineering Science 97 (2013) 394–405

Contents lists available at SciVerse ScienceDirect

Chemical Engineering Science

journal homepage: www.elsevier.com/locate/ces

Front tracking simulation of cell detachment dynamic mechanism in microfluidics

Zheng Yuan Luo [a,b], Shu Qi Wang [c], Long He [a,b], Tian Jian Lu [b], Feng Xu [b,d,*], Bo Feng Bai [a,b,*]

[a] State Key Laboratory of Multiphase Flow in Power Engineering, Xi'an Jiaotong University, Xi'an 710049, PR China
[b] Biomedical Engineering & Biomechanics Center, Xi'an Jiaotong University, Xi'an 710049, PR China
[c] HST-Center for Biomedical Engineering, Department of Medicine, Brigham and Women's Hospital, Harvard Medical School, Boston, MA, 02139, USA
[d] MOE Key Laboratory of Biomedical Information Engineering, School of Life Science and Technology, Xi'an Jiaotong University, Xi'an 710049, PR China

HIGHLIGHTS

- A model based on front tracking method was developed for cell detachment dynamic mechanism.
- We obtained several interesting events of cell adhesion: bonding, detachment and rebonding.
- Viscosities of cytoplasm and nucleus significantly affect cell attachment and detachment.
- Effects of shear stress, confinement and membrane elasticity on cell detachment were studied.

ARTICLE INFO

Article history:
Received 4 January 2013
Received in revised form
7 April 2013
Accepted 18 April 2013
Available online 29 April 2013

Keywords:
Biomedical engineering
Mathematical modeling
Multiphase flow
Simulation
Cell detachment
Microfluidics

ABSTRACT

Selective capture of target cells from whole blood in microfluidic systems is essential for clinical diagnosis and basic research (*e.g.,* genomic and proteomic characterization). However, the efficiency of capturing rare cells such as circulating tumor cells or stem cells via microfluidic systems is low. Although studies have shown that increasing wall shear stress can reduce cell capture efficiency, the underlying mechanisms are not yet clear. Here, we developed a theoretical model to understand how parameters such as shear stress, cell properties and microchannel height affect cell detachment, which is a key factor causing reduced cell capture efficiency. In this model, we used a front tracking method to track cell deformation and calculate elastic force acting on cell membrane. We also employed adhesion dynamic simulation to calculate the adhesion force between capturing agents (*e.g.,* antibody) and target cells. With these two methods, we simulated cell detachment under parabolic shear flows and investigated effects of mechanical parameters (shear stress, viscosities of cytoplasm and nucleus, elastic properties of cell membrane) and the ratio of cell radius to microchannel height on cell detachment. Cell detachment rate increased exponentially with increasing wall shear stress. In addition, a higher viscosity of intracellular fluid results in lower critical wall shear stress for cell detachment, dramatically reducing cell detachment rate. Microchannel height did not significantly affect cell detachment, especially when the ratio of cell radius to channel height is below 0.1. These results indicate the capability of the developed theoretical model to improve the design of microfluidic systems and operation conditions to reduce cell detachment, and thus improve cell capture efficiency.

1. Introduction

Separation and enumeration of cellular components from blood is essential for diagnosing and monitoring disease treatment (Phillips et al., 1991; Smerage and Hayes, 2006). Inspired by cell adhesion in blood vessels, microchannels immobilized with antibody have been developed to capture and count cells, such as CD4 +T cells for monitoring antiretroviral therapy in AIDS patients (Cheng et al., 2007; Cheng et al., 2009), and circulating tumor cells (CTCs) for early diagnosis in cancer patients (Nagrath et al., 2007; Stott et al., 2010a, 2010b). In general, microfluidics-based cell capture/quantification involves four main steps, *i.e.,* immobilization of specific antibodies onto the microchannel surface, injection of whole blood into the microchannels to capture target cells, removal of non-target cells by washing, and enumeration or further characterization of the captured target cells. This testing

* Corresponding authors at: State Key Laboratory of Multiphase Flow in Power Engineering, Xi'an Jiaotong University, Xi'an 710049, PR China. Tel.: +86 29 82665316; fax: +86 29 82669033.
E-mail addresses: fengxu@mail.xjtu.edu.cn (F. Xu), bfbai@mail.xjtu.edu.cn (B.F. Bai).

0009-2509/$ - see front matter © 2013 Elsevier Ltd. All rights reserved.
http://dx.doi.org/10.1016/j.ces.2013.04.038

protocol is simple and eliminates the need for peripheral equipment such as flow cytometry (Huh et al., 2005), offering great potential for point-of-care (POC) diagnostic applications. However, the low capture efficiency of target cells with microfluidics significantly limits its usage in clinical settings, especially for low target cell concentrations such as rare CTCs in the presence of an overwhelming number of other cellular components (*e.g.*, red blood cells).

Enduring efforts have been devoted to investigate the physical mechanisms underlying the low cell capture efficiency of microfluidic systems (Murthy et al., 2004; Sin et al., 2005; Plouffe et al., 2008). It is revealed that the capture efficiency is significantly reduced with increasing wall shear stress (*e.g.*, due to increased flow rate) using a Hele-Shaw device (Murthy et al., 2004; Cheng et al., 2007; Nagrath et al., 2007). Under the same wall shear stress, the cell capture efficiency may vary among different cell types (*e.g.*, CD4+T cells and monocytes) (Cheng et al., 2007; Cheng et al., 2009). Besides, channel height is also found to affect the cell capture efficiency. It has been demonstrated that the capture efficiency of PC3 prostate cancer cells decreases by ~25% when the channel height of a herringbone-chip is increased from 50 μm to 150 μm (Stott et al., 2010a). During the process of cell capture and separation with antibody-based microfluidics, the movement of target cells in functionalized microchannels (Fig. 1a) includes cell capture, cell rolling and cell detachment. To improve the capture efficiency, operating conditions including flow rate and channel height may be optimized to increase cell capture while reducing cell detachment. Recent experiments and statistical fitting data demonstrated that the number of detached cells increased exponentially with increasing shear stress (Decave et al., 2002; Zhang et al., 2008; Cheung et al., 2009), indicating that cell detachment negatively affects capture efficiency. Therefore, it is critical to understand the underlying physical mechanisms of cell detachment in microchannels.

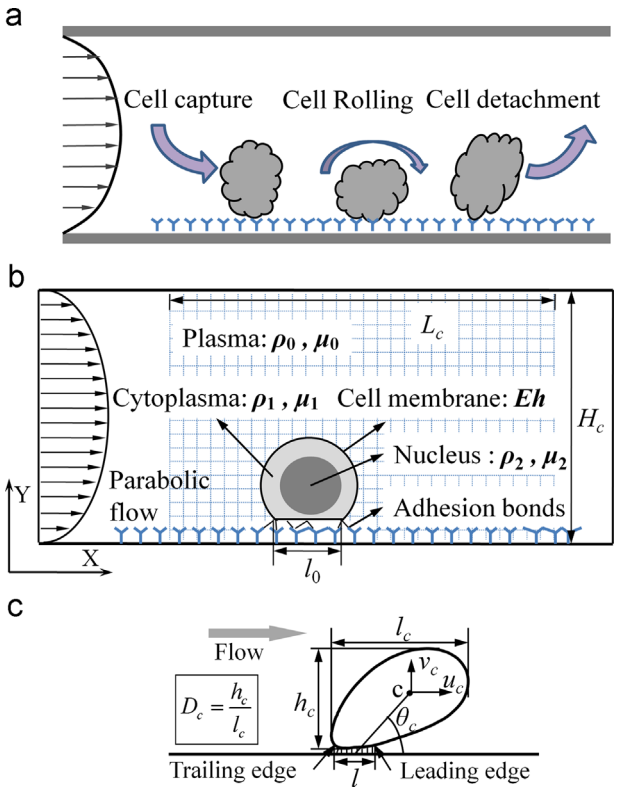

Fig. 1. Illustration of problem statement. (a) Actual cell movement in functionalized microchannel including cell capture (binding to antibody), cell rolling and cell detachment (being washed away). (b) Simplified theoretical model of cell detachment, where the deformable cell is considered as a compound drop surrounded by an elastic membrane (cell membrane) with two fluid parts (cytoplasm and nucleus). The cell initially adheres to the functionalized bottom surface with initial contact area of l_0. (c) Schematic of selected parameters including deformation parameters D_c and θ_c, velocity of cell center (u_c in X-axis direction and v_c in Y-axis direction) and transient adhesion area l.

A number of mathematical models have been developed to simulate the cell adhesion process in microfluidic systems (Verdier et al., 2009; Bai et al., 2013a), including the adhesive dynamic algorithm for shear threshold effect on cell adhesion and rolling (Chang et al., 2000; King and Hammer, 2001a,b; Caputo et al., 2007), the volume of fluid (VOF) method for cell deformation and tether (Khismatullin and Truskey, 2004, 2005), and the immersed boundary method for cell deformation and "stop-and-go" rolling motion (Kan et al., 1999; Jadhav et al., 2005; Pappu and Bagchi, 2008; Pappu et al., 2008). However, these models focused mainly on cell adhesion and deformation, although the understanding of cell detachment is also important for cell adhesion based microfluidics. An nano-to-micro scale adhesive dynamic algorithm by King et al. and a boundary integral method by Cantat and Misbah were developed to study dynamical unbinding of adhering vesicles and tethered leukocytes under a shear flow (Cantat and Misbah, 1999; King et al., 2005). However, cell deformation was neglected in the nano-to-micro scale adhesive dynamic algorithm by King et al., and the captured cells were assumed to be exposed to a simple shear flow in the boundary integral method by Cantat and Misbah. Besides, the underlying mechanisms for the effects of several mechanical parameters on cell detachment in microchannels are missing, *e.g.*, shear stress, intracellular fluid viscosities, elastic properties of cell membrane and the confinement (the ratio of cell radius to microchannel height). There is still an unmet need for an effective mathematical model to understand cell detachment in microfluidic systems.

Here, we established a mathematical model to simulate cell detachment behavior in microchannels. The prediction from the mathematical model revealed that increasing wall shear stress exponentially increased cell detachment, whereas increasing intracellular fluid viscosity and channel height significantly reduced cell detachment. The model presented in this study provides insights to develop cell-based microfluidic devices for POC testing.

2. Computational methods

2.1. Flow configuration

According to the movement of target cells in microfluidics (Fig. 1a), we established a theoretical model (Fig. 1b) to study cell detachment from a functionalized surface in a parabolic flow (the typical flow pattern in microfluidics) between two parallel plates with a distance H_c. In this model, the deformable cell is considered as a compound drop (cytoplasm and nucleus) surrounded by an elastic membrane (cell membrane). The whole fluid system is divided into three parts: a suspending fluid (plasma) and two fluids in the cell (cytoplasm and nucleus), which all behave as Newtonian fluid with density and dynamic viscosity of ρ_0, μ_0, ρ_1, μ_1 and ρ_2, μ_2, respectively. Deformable microvilli (ruffles on cell membrane) are distributed uniformly over the cell membrane. Adhesion bonds are only allowed to form between receptors on microvilli tips and ligands functionalized on the channel bottom surface. The cell initially adheres to the bottom surface with an initial contact area of l_0.

Velocity and pressure are solved only over the computational domain with length L_c and height H_c. The XY coordinate system is set as: the main flow direction along the two plates is positive

Table 1
Parameter values used in the present study.

Parameter	Definition	Range	Reference	Value used
R (μm)	Cell radius	3.5∼7	Geissmann et al. (2003) and Luo et al. (2011b)	6.5
L_c (μm)	Channel length			$10R$
H_c (μm)	Channel height			$3R\sim12R$
k (s^{-1})	Shear rate			500∼4000
ρ_0 (kg/m^3)	Plasma density			1000
μ_0 (mPa s)	Plasma viscosity	0. 8∼1.2	Khismatullin and Truskey (2004), Jadhav et al. (2005), Khismatullin and Truskey (2005) and Pawar et al. (2008)	0.8
$\lambda_\rho=\rho_1/\rho_0$	Density ratio	1.06∼1.10	Geissmann et al. (2003) and Luo et al. (2011a,b)	1.08
$\lambda_\mu=\mu_1/\mu_0$	Viscosity ratio			1∼16
Eh (μN/m)	Membrane stiffness	25∼3000	Jadhav et al. (2005), Pappu et al. (2008),	25∼2500
N_l (μm^{-2})	Ligand density	$(5\sim50)\times10^3$	Bell (1978), Vonandrian et al. (1995) and Khismatullin and Truskey (2005)	1.0×10^4
N_r (μm^{-2})	Receptor density	$(0.5\sim5)\times10^3$	Bell (1978), Vonandrian et al. (1995) and Khismatullin and Truskey (2005)	1.0×10^3
k_{f0} (m^2/s)	Unstressed forward rate	10^{-11}	Chesla et al. (1998) and Khismatullin and Truskey (2005)	10^{-11}
k_{r0} (s^{-1})	Unstressed reverse rate	1.0	Chesla et al. (1998) and Khismatullin and Truskey (2005)	1.0
k_b (pN/μm)	Bond spring constant	500∼10000	(Dembo et al. (1988), Fritz et al. (1998) and Khismatullin and Truskey (2005)	5300
k_{ts} (pN/μm)	Transition spring constant	48∼950	Dembo et al. (1988), N'Dri et al. (2003) and Khismatullin and Truskey (2005)	100
k_{mv} (pN/μm)	Microvillus spring constant	152∼1340	Park et al. (2002) and Khismatullin and Truskey (2005)	210
r_{mv} (μm)	Microvillus radius	0.1	Bell (1978), Shao et al. (1998) and Khismatullin and Truskey (2005)	0.1
l_{mv0} (μm)	Unstressed microvillus length	0.05∼1.0	Bruehl et al. (1996)	0.5
l_{b0} (μm)	Unstressed bond length	0.1	Fritz et al. (1998) and Khismatullin and Truskey (2005)	0.1
k_{bo} (Nm/K)	Boltzmann constant			1.4×10^{-23}
T (K)	Temperature			310.0

direction of the X-axis and the direction vertically pointing to the upper plate is positive direction of the Y-axis. Under steady-state conditions, the fluid velocity in the absence of cells is governed by a parabolic profile for plane Poiseuille flows. The parameter values used in this study are taken from our previous studies (Luo et al., 2011a,b) and literatures, as listed in Table 1.

2.2. Front tracking method

To simulate cell detachment in microchannels, we need an appropriate method to compute the time-dependent flow field and track cell deformation induced by the shear stress. Cell deformation may increase the contact area between the captured cell and functionalized channel surface during cell adhesion and rolling (Dong et al., 1999; Jadhav et al., 2005; Khismatullin and Truskey, 2005). Therefore, it is important to consider cell deformation during detachment. The adhesive dynamic algorithm (Chang et al., 2000; King et al., 2005; Caputo et al., 2007) assumes the cell as a rigid sphere and cannot capture the cell deformation. Several multiphase flow simulation methods, *e.g.*, the volume of fluid method (VOF) (Khismatullin and Truskey, 2004, 2005) and level set method (LS) (Luo et al., 2011a,b), consider cells as droplets surrounded by interfaces with a constant surface tension, then the effects of cell deformation can be easily included. However, the elastic properties of cell membrane, which is hard to be included in VOF and LS, contribute significantly to cell deformation in shear flows (Eggleton and Popel, 1998; N'Dri et al., 2003). Accordingly, we employed a front tracking method (FTM) to capture the moving interface, which is capable to consider the elastic properties of cell membrane and track the cell deformation (Unverdi and Tryggvason, 1992; Tryggvason et al., 2001) (Fig. 2a). In this method, a single set of conservation equations is used to solve the whole flow field (including both the intracellular and extracellular fluid). The governing equations to describe the conservation of mass and momentum of the incompressible flow system

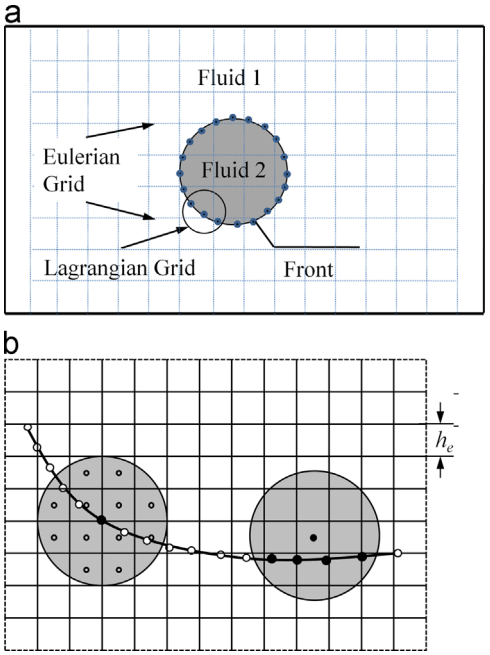

Fig. 2. The basic principle of front tracking method. (a) The fluid (Eulerian grid) is separated by the moving interface (Lagrangian grid). (b) Grid nodes (covered by a sphere of radius $2h_e$ surrounding the target grid node) contributing to the computation of quantity transfer between Eulerian grid and Lagrangian grid.

are

$$\nabla\cdot\boldsymbol{u}(\boldsymbol{x},t)=0 \tag{1}$$

$$\rho(\boldsymbol{x},t)\left[\frac{\partial\boldsymbol{u}(\boldsymbol{x},t)}{\partial t}+\boldsymbol{u}(\boldsymbol{x},t)\cdot\nabla\boldsymbol{u}(\boldsymbol{x},t)\right]=-\nabla p(\boldsymbol{x},t)+\boldsymbol{F}(\boldsymbol{x},t)$$
$$+\nabla\cdot[\mu(\boldsymbol{x},t)(\nabla\boldsymbol{u}(\boldsymbol{x},t)+\nabla^T\boldsymbol{u}(\boldsymbol{x},t))] \tag{2}$$

where $\boldsymbol{x}$ and $\boldsymbol{u}$ are vectors of the position and velocity, t and p are the time and pressure, ρ and μ are the fluid density and viscosity whose values depend on $\boldsymbol{x}$ and t, and $\boldsymbol{F}$ is the source term of total forces acting on cell membrane, *i.e.,* elastic force $\boldsymbol{f_e}$ due to cell deformation and adhesion force $\boldsymbol{f_a}$ due to adhesion bond formation.

One key step in the front tracking method is to transfer information between Eulerian grids and Lagrangian points, *i.e.,* interpolation of fluid velocity onto cell membrane and distribution of forces acting on cell membrane to fluid Eulerian grids. The delta function was employed to realize the transfer, as

$$\boldsymbol{u}(\boldsymbol{x}',t) = D(\boldsymbol{x}-\boldsymbol{x}')\boldsymbol{u}(\boldsymbol{x},t) \tag{3}$$

$$\boldsymbol{F}(\boldsymbol{x},t) = D(\boldsymbol{x}-\boldsymbol{x}')\boldsymbol{F}(\boldsymbol{x}',t) = D(\boldsymbol{x}-\boldsymbol{x}')(\boldsymbol{f_e}(\boldsymbol{x}',t)+\boldsymbol{f_a}(\boldsymbol{x}',t)) \tag{4}$$

where $\boldsymbol{x}'$ is the position vector of points on the cell membrane, and $D(\boldsymbol{x}-\boldsymbol{x}')$ is a two-dimensional (2D) delta function, which is a product of multiplying two one-dimensional (1D) delta functions as

$$D(\boldsymbol{x}-\boldsymbol{x}') = \delta(x-x')\delta(y-y') \tag{5}$$

In the calculations, the 1D delta function is discretized as (Unverdi and Tryggvason, 1992; Tryggvason et al., 2001)

$$\delta(x-x') = \begin{cases} \frac{1}{4h_e}\left(1+\cos\left(\frac{\pi(x-x')}{2h_e}\right)\right) & for \quad |x-x'| \le 2h_e \\ 0 & for \quad |x-x'| > 2h_e \end{cases} \tag{6}$$

where h_e is the Eulerian grid size. With this discrete delta function, the quantity transfer between Eulerian grid and Lagrangian point is performed over a sphere of radius equal to $2h_e$ surrounding each grid node (Fig. 2b).

With the velocity interpolated from the fluid velocity at Eulerian grids, the position of cell membrane is advected as

$$\frac{d\boldsymbol{x}'}{dt} = \boldsymbol{u}(\boldsymbol{x}',t) \tag{7}$$

Subsequently, as the cell membrane is advected to a new position, the fluid properties including density $\rho(\boldsymbol{x},t)$ and viscosity $\mu(\boldsymbol{x},t)$ need to be updated. An indicator function $I(\boldsymbol{x},t)$ with value 1 inside the cell and 0 outside the cell is defined and constructed from the known position of the cell membrane. The fluid properties can thence be evaluated by

$$\begin{aligned} \rho(\boldsymbol{x},t) &= \rho_0 + (\rho_1-\rho_0)I(\boldsymbol{x},t) \\ \mu(\boldsymbol{x},t) &= \mu_0 + (\mu_1-\mu_0)I(\boldsymbol{x},t) \end{aligned} \tag{8}$$

To find the indicator function, the following Poisson equation needs to be solved:

$$\nabla^2 I = \nabla\cdot G \tag{9}$$

where $G(\boldsymbol{x},t)$ is the gradient field calculated by:

$$G = \sum_l D(\boldsymbol{x}-\boldsymbol{x}^{(l)})\boldsymbol{n}^{(l)}\Delta s^{(l)} \tag{10}$$

Here, D is the discrete 2D delta function calculated by Eqs. (8) and (9) whilst $\boldsymbol{x}^{(l)}$, $\boldsymbol{n}^{(l)}$ and $\Delta s^{(l)}$ are the centroid, the unit normal vector to the cell membrane and the length of discrete line segment on the cell membrane, respectively. Details of the method can be found in articles by Tryggvason and co-workers (Unverdi and Tryggvason, 1992; Tryggvason et al., 2001).

2.3. Cell simulation

As previously mentioned, the cell was modeled as a viscous liquid capsule surrounded by an elastic membrane (cell membrane). When the nucleus is considered, a compound drop model was employed (Kan et al., 1999; N'Dri et al., 2003; Khismatullin and Truskey, 2004, 2005), where the cell including cytoplasm and nucleus is surrounded by an elastic membrane (cell membrane), with the nucleus occupying 44% of the cell volume (Schmidschonbein et al., 1980; N'Dri et al., 2003). Extracellular fluid induces cell deformation which in turn generates elastic force $\boldsymbol{f_e}$ on the cell membrane. The neo-Hookean model was introduced to compute the elastic force, due to its simplicity and ability to effectively capture the general characteristics of the cell (Jadhav et al., 2005; Pappu and Bagchi, 2008). The strain energy function of a 2D neo-Hookean membrane around a three-dimensional (3D) cell is given by

$$W = Eh\left(\varepsilon_1{}^2+\varepsilon_2{}^2+\frac{1}{\varepsilon_1{}^2\varepsilon_2{}^2}\right) \tag{11}$$

where E and h are the shear modulus of elasticity and thickness of the membrane; ε_1 and ε_2 are the principal stretch ratios. Then, the tension T_e on a 1D neo-Hookean membrane around a 2D cell can be computed by using the equation introduced by Bagchi and co-workers (Bagchi et al., 2005; Bagchi, 2007), as

$$T_e = \frac{Eh}{\varepsilon^{3/2}}(\varepsilon^3-1) \tag{12}$$

where ε is the stretch ratio of a discrete line segment, *i.e.,* undeformed length divided by deformed length. Then, the elastic force acting on any Lagrangian grid point on the membrane can be obtained from the tensions in two adjacent line segments denoted by i and j, as

$$\boldsymbol{f_e} = T_{ei}\boldsymbol{e_i}-T_{ej}\boldsymbol{e_j} \tag{13}$$

where $\boldsymbol{e_i}$ and $\boldsymbol{e_j}$ are the unit tangent vectors along the two line segments.

2.4. Cell adhesion simulation

Since receptors clustered at microvilli (ruffles on cell membrane) tips are responsible for cell adhesion (Vonandrian et al., 1995), microvillus deformation also affects cell adhesion as indicated by cell rolling research (Pawar et al., 2008). To introduce the effects of microvillus deformation on cell detachment, we developed a new adhesion dynamic model (ADM) that is more realistic compared to the microvillus-bond spring model used by Khismatullin and Truskey (2004, 2005). The microvilli were modeled as massless elastic cylinders, which distribute uniformly on the smooth cell membrane and have adhesion molecules (receptors) on their tips (Fig. 3a). Only receptors on microvilli tips have the chance to interact with their counterparts (ligands) distributed uniformly on the bottom functionalized channel surface. Besides, adhesion bonds form between the microvillus tip and the bottom surface, if and only if the separation distance between them does not exceed the unstressed bond length l_{b0}.

Whilst the adhesion bonds behave as Hookean springs with spring constant k_b, the microvilli are taken as springs with spring constant k_{mv} to account for their deformability. The microvillus and bonds formed on its tip are assumed to be aligned in the same direction (Khismatullin and Truskey, 2004). In the model used by Khismatullin and co-workers (Khismatullin and Truskey, 2004, 2005), the microvillus spring and the adhesion bond spring were integrated into one new spring (microvillus-bond spring) characterized by an efficient spring constant $k_s = k_b k_{mv}/(k_b+k_{mv})$, Fig. 3b. However, as k_b and k_{mv} may be different by two magnitude levels (see Table 1), we do not use this microvillus-bond spring method but treat the microvillus and bond separately (microvillus and bond springs model in Fig. 3b).

Once the separation distance between the microvillus tip and the functionalized bottom surface becomes less than or equal to the unstressed bond length l_{b0}, there forms a linkage between the microvillus and the functionalized surface. Then, the bond density N_b and the total adhesion force $\boldsymbol{f_a}$ acting on the microvillus may be

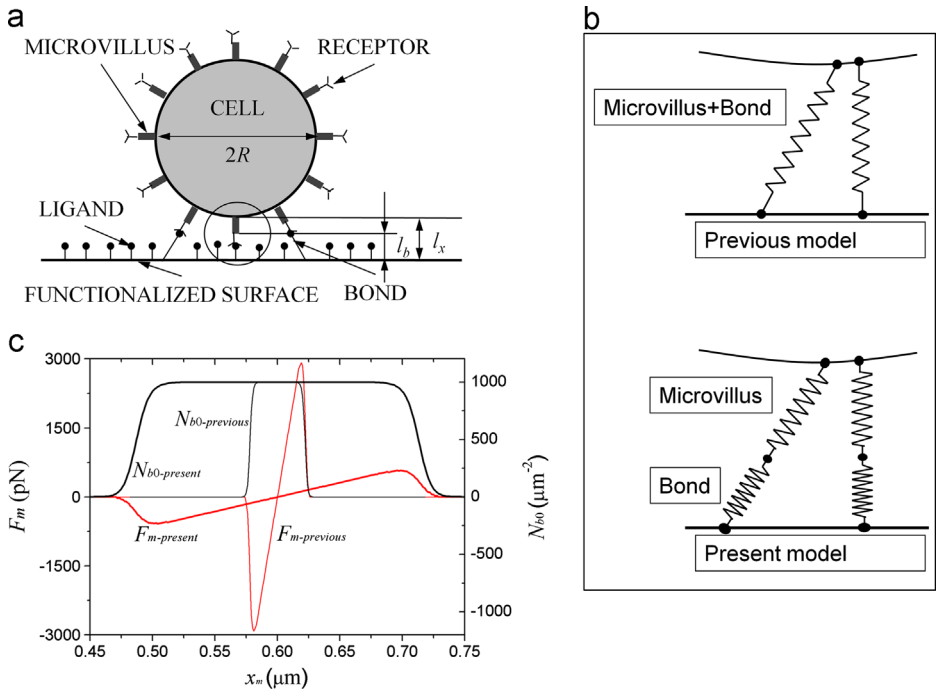

Fig. 3. Illustration of cell adhesion model. (a) Microvilli are modeled as massless elastic cylinders distributed uniformly on the smooth cell membrane. Only receptors on microvilli tips have the chance to interact with their counterparts (ligands) distributed uniformly on the bottom functionalized surface. (b) Microvillus and adhesion bond are integrated into one spring (microvillus-bond spring) with an efficient spring constant in a previous model (Khismatullin and Truskey, 2004, 2005), whilst they are treated as two separate springs in this article (present model). (c) Variation of equilibrium bond density and total adhesion force on single microvillus in different adhesion models (calculated by using the method of Jin et al. (2007)), which indicates our adhesion model is more stable than the previous model.

calculated using a kinetic model developed by Dembo et al. (1988), as

$$\frac{dN_b}{dt} = k_f(N_l - N_b)(N_r - N_b) - k_r N_b \tag{14}$$

where N_r and N_l are separately receptor density on the microvillus and ligand density on the functionalized surface, and k_f and k_r are the forward and reverse reaction rate coefficients computed by

$$k_f = k_{f0}\exp\left[-\frac{k_{ts}(l_b - l_{b0})^2}{2k_{bo}T}\right]$$

$$k_r = k_{r0}\exp\left[-\frac{(k_b - k_{ts})(l_b - l_{b0})^2}{2k_{bo}T}\right] \tag{15}$$

Here, k_{f0} and k_{r0} are the unstressed forward and reverse reaction rate coefficients; k_{ts} is a transition spring constant of adhesion bonds at the state changing from slip bonds to catch bonds; l_{b0} is the length of unstressed bond; k_{bo} and T are the Boltzmann constant and absolute temperature respectively. When the deformable microvillus and adhesion bond are separately considered as two springs, the bond length l_b can be calculated by

$$l_b = \frac{k_{mv}(l_x - l_{mv0}) + k_b l_{b0}}{k_{mv} + k_b} \tag{16}$$

where l_{mv0} and l_{b0} are the lengths of unstressed microvillus and bond; l_x is the separation distance between the cell membrane (microvillus base) and the functionalized surface. When linkage forms between one microvillus and the functionalized surface, the position of the microvillus base is stored as x_b. Then l_x can be computed by

$$l_x = \sqrt{(x_{mv} - x_b)^2 + {y_{mv}}^2} \tag{17}$$

where x_{mv} and y_{mv} characterize the new position of the microvillus base.

Once the bond density on microvilli is obtained, the number n_b of adhesion bonds on every microvillus can be calculated as

$$n_b = N_b S_{tip} = N_b \pi {r_{mv}}^2 \tag{18}$$

where r_{mv} and S_{tip} are the radius of the microvillus and the surface area of the microvillus tip respectively. If n_b becomes less than unity, the linkage between the microvillus and the functionalized surface is broken. If not, the adhesion force $\boldsymbol{f_a}$ acting on the cell membrane can be computed by

$$\boldsymbol{f_a} = n_b k_b (l_b - l_{b0})\boldsymbol{I} \tag{19}$$

where $\boldsymbol{I}$ (I_x, I_y) is the unit vector directed from the microvillus base to the functionalized surface, with

$$I_x = \frac{(x_b - x_{mv})}{l_x}$$

$$I_y = \frac{-y_{mv}}{l_x} \tag{20}$$

The values of the parameters used in this article, see Table 1, are based on the data of real leukocytes.

For a specific position of the microvillus base (a given l_x), the equilibrium bond density N_{b0} can be calculated, which varies only with the separation distance l_x other than the time. In order to compare the two aforementioned models for microvillus deformability, the equilibrium bond density and the resultant adhesion force on one microvillus tip are computed (Fig. 3**c**) using the method of Jin et al. (2007). The microvillus-bond spring model predicts much sharper adhesion force (larger value over a smaller range), which may induce numerical instability near the cell membrane.

2.5. Numerical resolution and code

The cell detachment under shear flow in a microchannel bounded by two parallel plates was simulated using the mathematical model presented in previous sections. The undeformed

cell was assumed to have a circular shape with initial contact area $l_0=R$ (Cheung et al., 2009; Couzon et al., 2009) on the bottom functionalized surface (Fig. 1**b**). The fluid in the microchannel was assumed to be stationary initially. Non-slip boundary conditions were applied to the surfaces of the two parallel plates. The parabolic velocity profile of Eq. (1) was employed as the boundary condition at the inlet.

The governing equations were normalized to be solved with characteristic quantities, *i.e.*, length R, velocity kR, time $1/k$. A two-step time-split scheme with second-order accuracy (Projection method) was employed to solve the Navier–Stokes equations (Eqs. (4) and (5)) of unsteady incompressible flow. In this method, the momentum equation (Eq. (5)) was split into a convection–diffusion equation and a pressure Poisson equation (PPE), which were used to solve the flow velocities and the pressure field, respectively. The convection–diffusion equation was solved firstly to calculate the intermediate velocities, which are not divergence-free and used to update the PPE. The pressure field were computed by solving the updated PPE and then used to correct the velocities to make them divergence-free. The 2D numerical simulation of cell detachment in microfluidics was carried out by our own incompressible computational fluid dynamics (CFD) code.

The temporal accuracy was ensured to be second order by the projection method for unsteady flow. The governing equations were all spatially discretized using a second order difference scheme (the standard central difference scheme). The Crank–Nicholson semi-implicit technique was used to update the diffusion term for stability, whilst the Adams–Bashforth method was employed to update other terms including advection, pressure and body force. The ADI (alternating direction implicit) scheme and multi-grid techniques were employed to solve the PPE. The cell membrane advection equation was solved using the Adams–Bashforth method. The fourth-order Runge–Kutta method was used to solve the adhesion kinetics equation to obtain bond density on each microvillus, with initial bond density set as the aforementioned equilibrium bond density N_{b0}.

3. Model validation and simulation results

To validate our numerical code with the front tracking method, we simulated the deformation of an initially circular cell in linear shear flow (Fig. 4a). The flow was bounded by two parallel moving plates with separation distance H_c. No-slip condition was imposed at the upper and bottom plates, with the upper one moving in the positive direction of X-axis and the bottom one in the opposite direction at the same constant velocity. Periodic conditions were imposed at the other boundaries in the X-axis direction. The cell was initially placed in the middle of the computational domain with length $10R$ and height $10R$. The dimensionless stiffness of the cell membrane was defined as $G=\mu_0 kR/Eh$.

The tank-treading motion of the cell in linear shear flow is captured by our model, as shown in Fig. 4. The cell deforms from the initial circular shape to elliptical shape and maintains it as a steady state, whilst the cell membrane is still rotating around intracellular fluid driven by the shear force of the surrounding fluid. This behavior was also observed for red blood cells in previous experiments by Fischer et al. (1978). As the stiffness of cell membrane is increased, the cell deformation decreases, *i.e.*, decreasing of deformation index D and inclination angle θ in Fig. 4b and c, which is qualitatively consistent with previous numerical simulation results (Eggleton and Popel, 1998; Ramanujan and Pozrikidis, 1998; Breyiannis and Pozrikidis, 2000). Besides, we quantitatively compared the process of cell

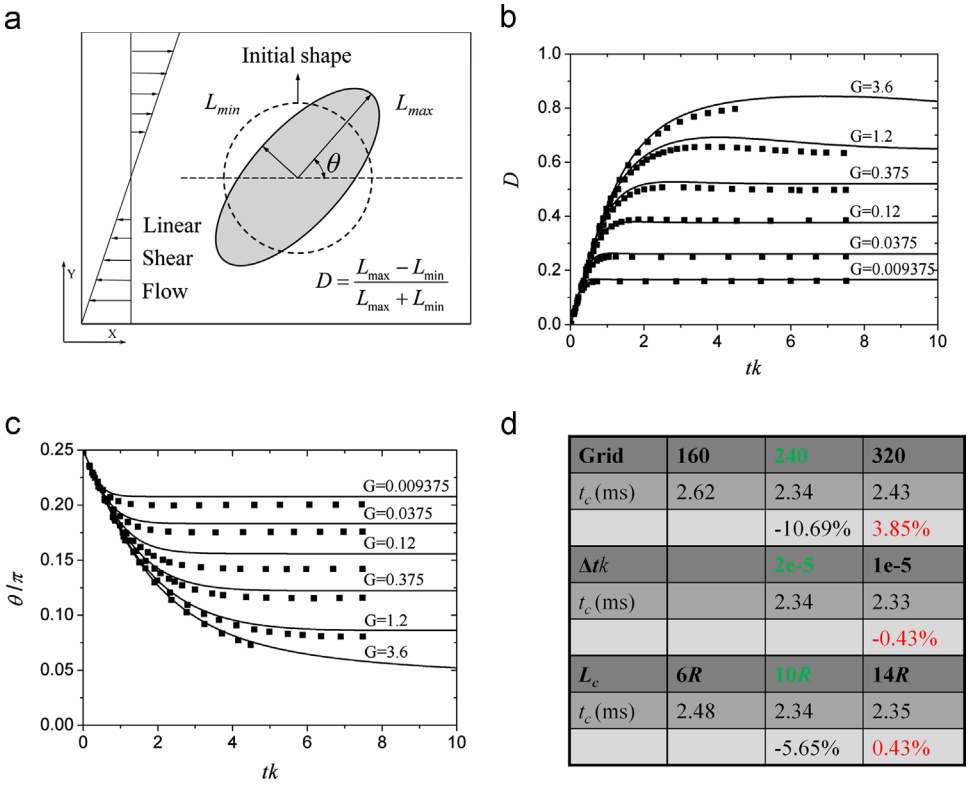

Grid	160	240	320
t_c (ms)	2.62	2.34	2.43
		-10.69%	3.85%
Δtk		2e-5	1e-5
t_c (ms)		2.34	2.33
			-0.43%
L_c	$6R$	$10R$	$14R$
t_c (ms)	2.48	2.34	2.35
		-5.65%	0.43%

Fig. 4. Validation of the computational fluid dynamics (CFD) code. (a) The deformation of an initially circular cell in linear shear flow is used to validate our CFD code. (b) and (c) are deformation index D and inclination angle θ plotted as functions of time. The solid line denotes the present results and the square dots are taken from the literature (Breyiannis and Pozrikidis, 2000). Results are shown for selected values of dimensionless stiffness of the cell membrane G, which match very well. (d) Resolution test for grid, time step and channel length. The length $10R$ for computational domain, time step $\Delta t_k=2e\text{-}5$ and mesh size 240 for channel height $6R$ are sufficient for tracking cell deformation and detachment.

deformation predicted by our model with numerical results obtained by Breyiannis and Pozrikidis (Breyiannis and Pozrikidis, 2000) with boundary integral simulation for the Stokes flow. The largest discrepancy of deformation index D between our results and Breyiannis's was only 4.6% for all the range of G. This small discrepancy is attributed to the fact that the model employed by Breyiannis and Pozrikidis ignored inertia effects, as inertia may affect cell deformation in shear flows (Sui et al., 2009; Bai et al., 2013b). The simulation of cell detachment was performed using a mesh density of 40 for one cell radius with time step Δt_k=2e−5 and computational domain length L_c= 10R. It has been established that more dense meshes and smaller time steps contribute little but consume much more computing resources and, with the computational domain length fixed at L_c=10R, the inlet and outlet boundary conditions have small influence on cell detachment, Fig. 4d.

Next, we simulated cell detachment with membrane stiffness Eh=250 μN/m and cytoplasm viscosity $\mu_1=2\mu_0$ in a microchannel flow of k=2000 s^{-1} and H_c=6R. The snapshots of cell shape predicted at different time points are presented in Fig. 5a. Induced by the cooperation of hydrodynamic forces and adhesion forces, the cell is elongated from the initial circular shape to a teardrop shape, which has been observed in previous cell rolling experiments (Dong et al., 1999; Zhang et al., 2008). Subsequently, whilst the cell maintains the teardrop shape with no obvious further deformation (constant D_c in Fig. 5d) it gradually rotates following the flow direction (decreasing θ_c in Fig. 5d). In this process, the cell membrane near the leading edge deviates from the initial curve and is flattened (also observed in firm adhesion and cell rolling researches (Jadhav et al., 2005; Khismatullin and Truskey, 2005)) due to the relatively high pressure region under the cell (Fig. 5b) shown by our own results as well as previous studies (Liu and Wang, 2004; Luo et al., 2011a). Shear stresses from the surrounding fluid generate translational drag force and rotating torque on the cell. As a result, the teardrop-shaped cell is pulled forward and the first linked microvillus (FLM) at the trailing edge is subjected to the most powerful force and hence detaches first (Fig. 5**c**). The adhesion force and the induced resistance torque provided mainly by the FLM balance the translational drag force and rotating torque. Therefore, when the FLM is broken, the cell rapidly accelerates to a higher velocity. Subsequently, the cell gradually slows down as a result of the increasing adhesion force of the new FLM at the trailing edge (Fig. 5e). Consequently, the cell is found to detach in a “stop-and-go” motion style similar to that found for cell

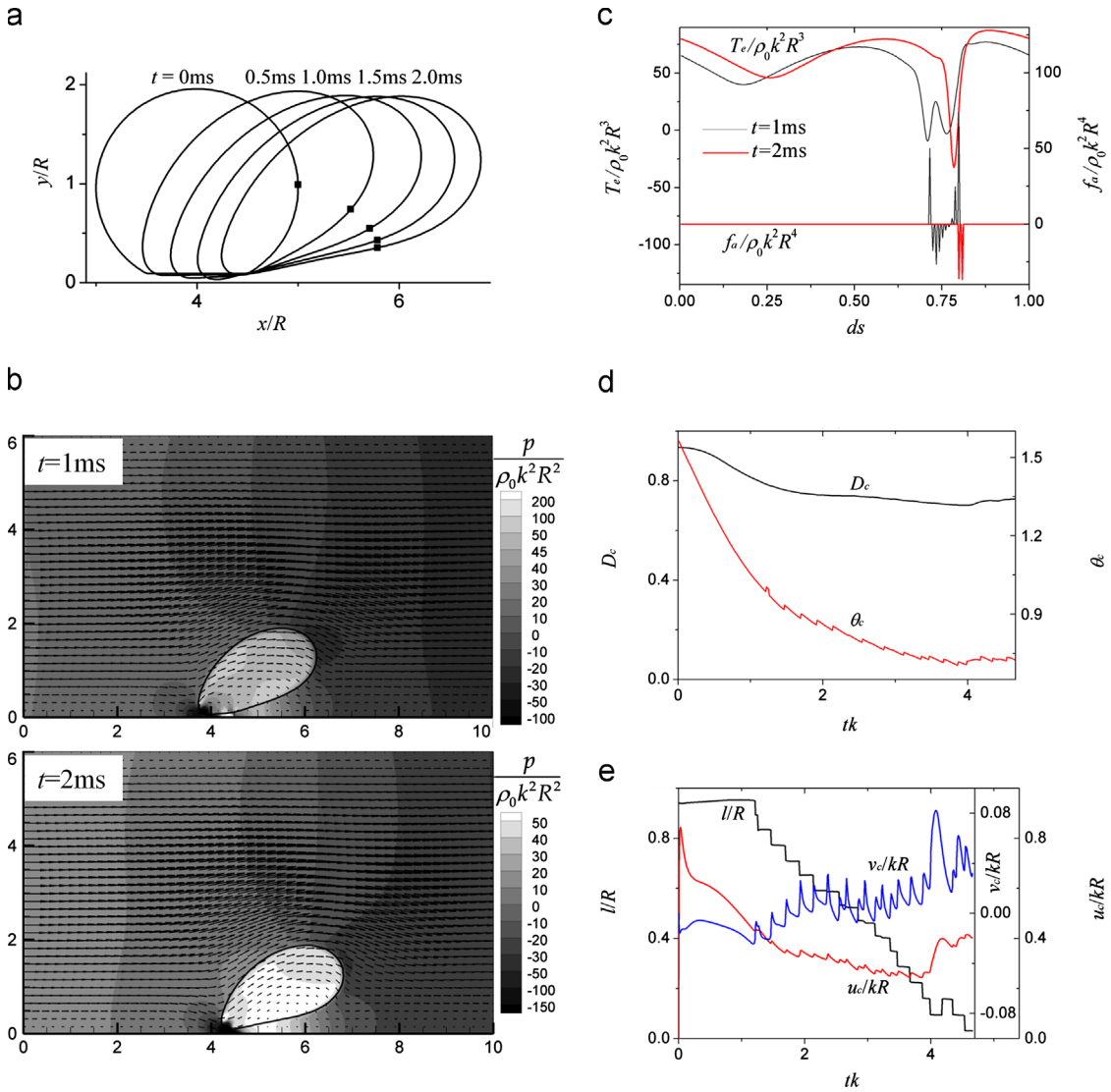

Fig. 5. Single cell detachment at control parameters of k=2000 s^{-1}, Eh=250 μN/m, μ_1/μ_0=2, H_c=6R. (a) Cell shape *versus* time. (b) Velocity vector and pressure field in the microchannel when t=1 ms and t=2 ms. (c) Elastic force and adhesion force along the counterclockwise direction of cell membrane, ds being the arc length along cell membrane. (d)Deformation parameters D_c and θ_c plotted as functions of time. (e) The velocity of cell center and transient adhesion area plotted as functions of time.

rolling (Jadhav et al., 2005; Pappu and Bagchi, 2008; Pappu et al., 2008). Nonetheless, the variability of cell transient velocity during cell detachment observed in the present study is much smaller than that during cell rolling (Fig. 5e).

Cell properties such as stiffness of cell membrane and viscosity of intracellular fluid (cytoplasm and nucleus) have significant effects on cell detachment, Fig. 6. Fig. 6b–c shows that decreasing membrane stiffness reduces membrane tension and enhances cell deformation, in accordance with existing numerical simulation results for cell deformation under linear shear flow conditions (Eggleton and Popel, 1998; Ramanujan and Pozrikidis, 1998). Cells with stiffer (Eh=2500 μN/m) or more flexible membrane (Eh=25 μN/m) detach faster than those with moderate membrane stiffness (Eh=250 μN/m), especially for relatively high wall shear stresses (*e.g.*, τ_w=1.6 Pa, Fig. 6a). Compared to cell membrane with Eh=25 μN/m, the membrane with Eh=250 μN/m provides larger pulling forces on the FLM, causing the bonds on the FLM near the trailing edge to detach faster (Fig. 6c). When the cell membrane stiffness is increased from Eh=250 μN/m to Eh=2500 μN/m, the stiffer membrane causes the cell to experience more rotating torque due to less deformation and larger translational drag force. Besides, a larger membrane stiffness (Eh=2500 μN/m) allows the cell to maintain its original circular shape so that the cell membrane near the leading edge is less flattened as described before (Fig. 6b). Hence, increasing the cell membrane stiffness (from Eh=250 μN/m to Eh=2500 μN/m) leads to increased bond formation rate on the microvillus near the leading edge, and slower cell detachment.

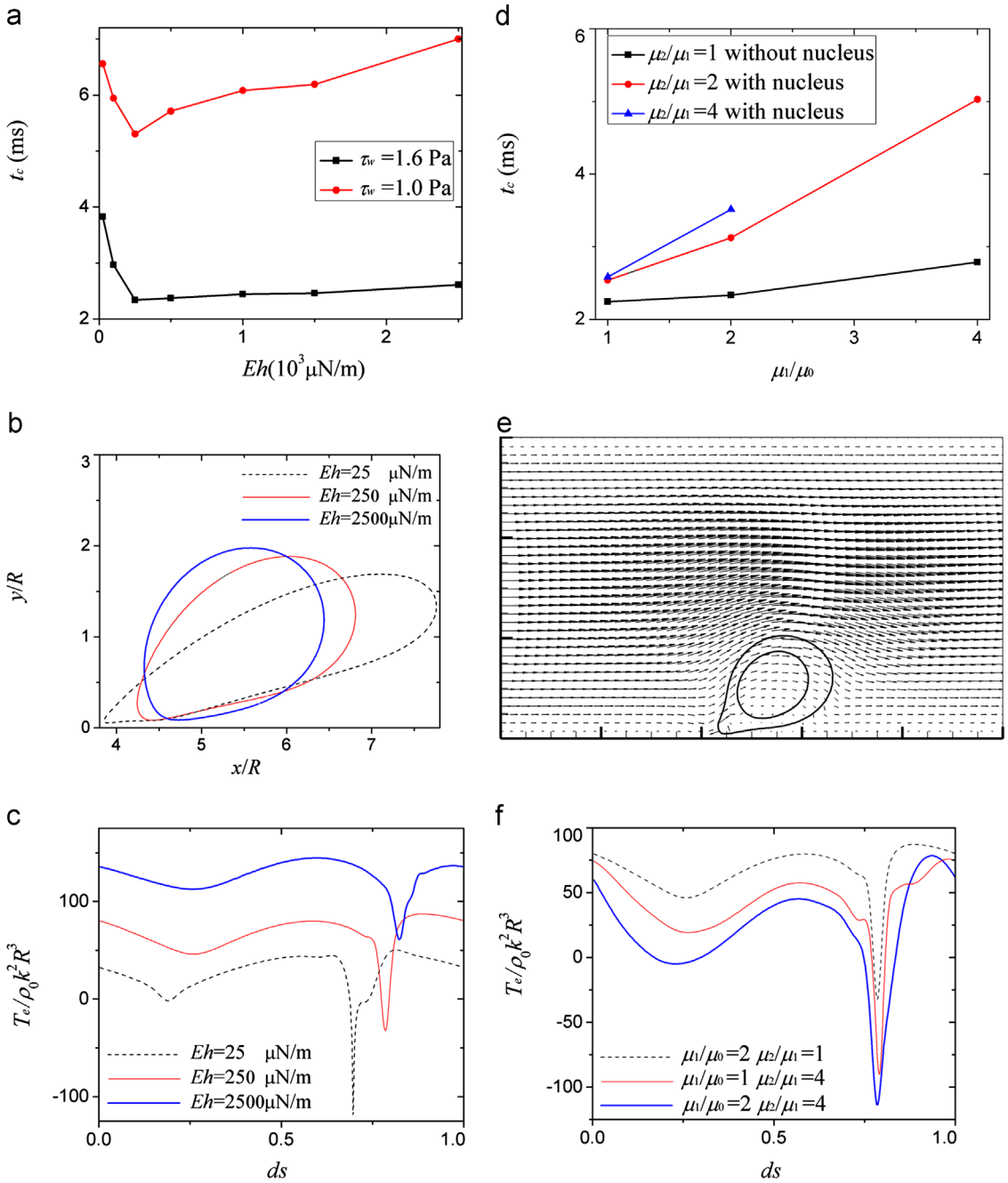

Fig. 6. Effects of cell properties on cell detachment. (a), (b) and (c) present the effects of cell membrane stiffness and (d), (e) and (f) present the effects of cell nucleus and intracellular fluid viscosity. (a) and (d) are the contact time plotted as a function of membrane stiffness Eh and intracellular fluid viscosity. (b) is the cell shape at t=2 ms and (e) is the cell shape and velocity vector at t=2 ms. (c) and (f) show elastic force along the counterclockwise direction of cell membrane at t=2 ms.

Under the same wall shear stress (τ_w=1.6 Pa), viscosities of intracellular fluid (cytoplasm and nucleus) have more significant effects on cell detachment than membrane stiffness (Fig. 6a and d). The cell with a relatively high intracellular fluid viscosity (μ_2:μ_1:μ_0=16:4:1) cannot be detached by the surrounding fluid and will roll continuously. The cell with a nucleus deforms and elongates significantly near the contact region (Fig. 6**e**) and then extends the microvillus length to resist cell detachment. Such fact known as cell tether is also observed in cell adhesion simulations and experiments (N'Dri et al., 2003; Khismatullin and Truskey, 2005). Hence, cells with nucleus are more difficult to be detached (Fig. 6d). Higher cytoplasm viscosities (*e.g.*, μ_1:μ_0=4:1) allow the cell membrane to maintain a larger curvature, enabling the microvillus near the leading edge to attach to the channel surface easier as mentioned before. Besides, membrane tension increases with increasing intracellular fluid viscosity, Fig. 6f. As higher membrane tensions correspond to higher dissociation rates of adhesion bonds at the trailing edge, increasing the intracellular fluid viscosity reduces cell detachment speed, Fig. 6d.

Cell detachment is found to increase exponentially with increasing wall shear stress (from τ_w=0.4 to 3.2 Pa) with or without flow acceleration, Fig. 7a. The cell cannot be detached from the functionalized surface when the wall shear stress is as low as 0.4 Pa. The flow with higher wall shear stress (*e.g.*, τ_w=3.2 Pa) in the same microchannel (H_c=6R) induces greater shear stress on cell membrane (Fig. 7d), which results in greater pulling force on the FLM and much faster dissociation of bonds near the trailing edge (Fig. 7b). However, whilst increasing the wall shear stress leads to increased translational drag force and cell deformation (Fig. 7c and d), there is no significant change of rotating torque on the cell. The bond formation rate of the microvillus at the leading edge is therefore not affected significantly by increased wall shear stress (Fig. 7b). As a result, cell detachment increases with increasing wall shear stress.

Cell detachment is less affected by microchannel height, as compared to flow condition and intracellular fluid viscosity. Cell contact time increases (from t_c=4.5 ms to t_c=6.0 ms) with increasing microchannel height (from H_c=4R to H_c=9R) for wall shear stress τ_w=1.0 Pa and initial contact area l_0=1.0R, Fig. 8a. The captured cell narrows the fluid channel and disturbs the flow of extracellular fluid, results in increased velocity gradient around the cell and increased shear stress on the cell according to the conservation of mass (Eq. (4)). The larger the ratio of cell radius to channel height is, the faster the fluid flows through a narrower fluid channel (Fig. 8d), leading to increased shear stress on the cell. As the shear stress is increase, both the detaching speed of the trailing edge (Fig. 8b) and the cell deformation increase (Fig. 8c). However, if the ratio of cell radius to microchannel height does not exceed 0.1, the presence of cell will not significantly affect the flow field and hence the cell detachment. However, as the channel height (H_c) is increased from 9R to 12R, the contact time (t_c) decreases from 6.0 ms to 5.5 ms (Fig. 8a), which is attributed to the process of establishing the steady-state flow. In this process, the cell deforms more quickly (Fig. 6c) and the trailing edge starts to detach earlier (Fig. 8b) when the channel height is increased from 9R to 12R, because the flow velocity around the cell is greater in the channel with a larger height to keep the wall shear stress constant (Fig. 8d). In contrast, cell detachment may not be affected by channel height under continuous flow conditions when the ratio of cell radius to channel height is less than 0.1.

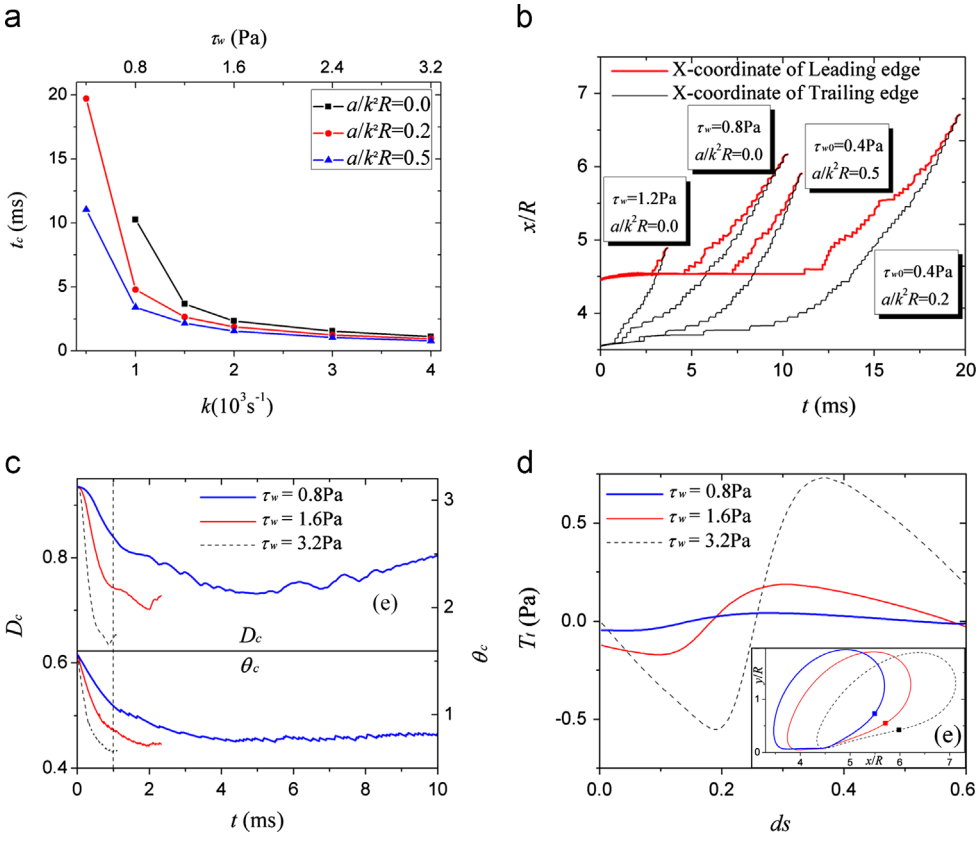

Fig. 7. Effects of flow condition on cell detachment. (a) Cell contact time plotted as a function of wall shear stress. (b) Positions of leading edge and trailing edge *versus* time. (c) Deformation parameters D_c and θ_c *versus* time at selected values of wall shear stress. (d) presents the tangential stress T_t acting on cell membrane along its counterclockwise direction. (e) Cell shape at t=1 ms, with square dots representing points of ds=0.0 in (d).

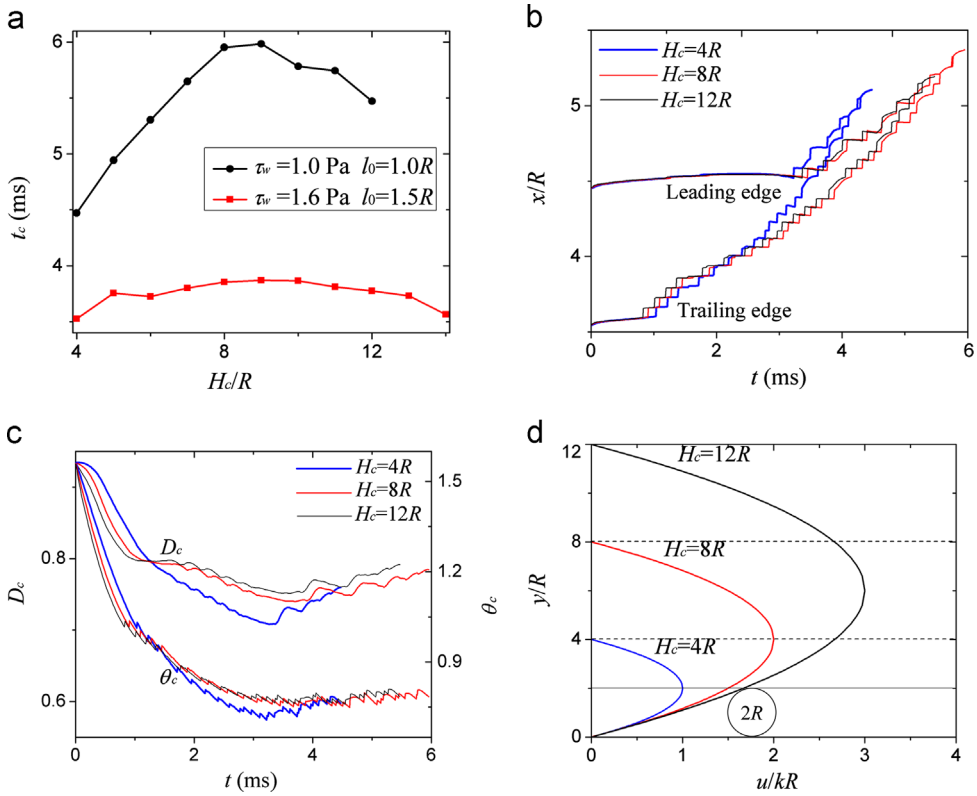

Fig. 8. Effects of channel height on cell detachment. (a) Contact time plotted as a function of channel height H_c. (b) Positions of leading edge and trailing edge plotted as functions of time at τ_w=1.0 Pa. (c) Deformation parameters D_c and θ_c *versus* time for selected values of channel height at τ_w=1.0 Pa. (d) Profile of inlet velocity in microchannel flow for selected values of channel height.

4. Discussion

In this study, a mathematical model integrating the front tracking method with cell adhesion dynamic simulation has been developed to investigate the mechanisms of cell detachment in microfluidics. Effects of several mechanical parameters (*e.g.*, shear stress, viscosities of cytoplasm and nucleus, elastic properties of cell membrane) and the confinement (ratio of cell radius to microchannel height) on cell detachment were investigated. During cell detachment, the cell is deformed from circular shape to teardrop shape by the surrounding flow and detached in "stop-and-go" style (Fig. 5). Our findings are consistent with previous cell rolling studies (Dong et al., 1999; Jadhav et al., 2005; Pappu and Bagchi, 2008; Zhang et al., 2008). Through including inertia and compound drop model, the presented model could be implemented for other theoretical applications, *e.g.*, inertial focusing phenomenon observed under laminar flow conditions in a microdevices (Di Carlo et al., 2007) and lateral migration of cells in microfluidics (Hur et al., 2011).

According to our simulation, the dissociation rate of bonds on the microvillus at the trailing edge and the forming rate of new bonds on the microvillus at the leading edge determine the total number of adhesion bonds between the cell and channel surface, thus controlling cell behaviors (*i.e.*, cell rolling and cell detachment). Increasing the wall shear stress increases the bond dissociation rate. When the bond dissociation rate is equivalent to the bond forming rate, the cell will keep rolling on the channel surface. When the wall shear stress exceeds a critical value, the bond dissociation rate becomes higher than the bond forming rate, leading to cell detachment. Correspondingly, when the wall shear stress exceeds the critical value, the cell detachment rate increases exponentially (Fig. 7), which is consistent with previous experimental studies (Zhang et al., 2008; Cheung et al., 2009). The present study also identifies cell detachment as the critical reason why the capture efficiency decreases greatly with increasing wall shear stress (Cheng et al., 2007; Nagrath et al., 2007).

Cell properties, especially the viscosity of intracellular fluid (including cytoplasm and nucleus), significantly affect cell detachment under shear flow conditions. The cell detachment rate doubles when the intracellular fluid viscosity is increased from μ_2:μ_1:μ_0=2:1:1 to μ_2:μ_1:μ_0=8:4:1. On the other hand, increasing the intracellular fluid viscosity increases the critical wall shear stress for cell detachment. The critical wall shear stress for cells with a higher intracellular fluid viscosity (μ_2:μ_1:μ_0=16:4:1) is greater than 1.6 Pa (Fig. 6). In comparison, experimentally it was revealed that the critical wall shear stress for cells ranges from 2 to 5 Pa (Couzon et al., 2009; Decave et al., 2002). The variation in the numerically predicted critical wall shear stress and that experimentally measured may be caused by the difference in cell properties between our cell model and real cells. The effect of wall shear stress on cell capture efficiency may vary, depending on the cell types (Cheng et al., 2007, 2009), since different types of cell may vary in cell properties such as intracellular fluid viscosity.

Channel height does not significantly affect cell detachment compared to wall shear stress and intracellular fluid viscosity, especially at low ratios (below 0.1) of cell radius to channel height (Fig. 8). The shear forces acting on the cell have no significant change at low ratios of cell radius to channel height (below 0.1) (Couzon et al., 2009). However, we cannot conclude channel height has little effect on cell capture efficiency, because cell separation is a multicellular process in real microfluidics and cells collide with each other frequently. For example, a smaller channel height provides more opportunity for cell to interact with channel surfaces, which can potentially increase cell adhesion.

Although our mathematical model reflected most important features of cell detachment, it still needs to be further developed.

The kinetic characteristic of adhesion bond plays an important role in adhesion forces, which may lead to different cell detachment rates. As cell separation is a multicellular process in real microfluidics and cells collide with each other frequently, the actual multicellular capture and separation from whole blood using microfluidic devices, the collisions and interactions between cells may increase cell detachment, which needs to be introduced into the mathematical model. The 2D model with circular cells actually simulated cylindrical cells in 3D flow. This limitation may lead to the difference between our simulation and the previous numerical study for the effects of channel height on cell deformation (Khismatullin and Truskey, 2004). Another limitation of our simulation is that the viscosity ratio of intracellular fluid to extracellular fluid was 16, which in reality can be more than 100 (Khismatullin and Truskey, 2004, 2005). The numerical instability of the Newtonian model limits the viscosity ratio of intracellular fluid to extracellular fluid at a low value, which is around unit in previous model (Cantat and Misbah, 1999; King et al., 2005) and is 16 in our model. Therefore, we suggest further developing numerical models to reveal the effects of the intracellular fluid viscosity on cell deformation, attachment and detachment in microfluidics. Besides, further development of mathematical models should include the effect of cell viscoelasticity (Khismatullin and Truskey, 2004, 2005), as cells change their mechanical properties, *e.g.*, the intracellular fluid viscosity, as a response to extracellular mechanical stimuli (Tsai et al., 1993), *e.g.*, shear stresses from shear flows.

Selective capture of target cells from whole blood is essential for basic researches and clinical diagnosis, such as capturing specific cell type for characterizations, separating and counting cells for disease diagnosis. The movement of cells from the mainstream to the functionalized surface is one of the major issues of cell capture, especially for capturing rare cells such as circulating tumor cells or stem cells. However, cell detachment is another critical factor to capture all target cells, when capture-based methods are used to separate and enumerate specific cells for disease diagnosis. To understand the physical mechanisms underlying cell detachment behaviors, we developed a mathematical model based on the front tracking method, which can be easily improved for other theoretical applications including the movement of cells from the mainstream to the surface. The effects of cell mechanical properties and the wall shear stress on cell detachment may partially interpret that the capture efficiency is significantly affected by the wall shear stress and cell type. This model and new insights from this study could be helpful for further design of capture-based microfluidics for biological applications, *e.g.*, the optimization of the channel structure and flow condition.

5. Conclusion

We developed a mathematical model to study cell detachment in microchannels. Our numerical results indicate that cell detachment is strongly dependent on the hydrodynamic flow field. Our major findings include: (1) the cell presents a tear-drop shape during cell detachment and exhibits a “stop-and-go” motion style; (2) cell detachment is strongly associated with the viscosity of intracellular fluid; (3) the cell detachment rate increases exponentially with increasing wall shear stress due to rapid bond dissociation at the trailing edge and insignificant change of bond formation rate at the leading edge; (4) the channel height does not affect cell detachment unless the ratio of cell radius to channel height exceeds 0.1. Our results indicate that our theoretical model is of value for understanding the parameters that can affect cell capture efficiency in microfluidic devices, which is essential to the design of microfluidics-based POC devices.

Nomenclature

H_c	Channel height as illustrated in Fig. 1, m
l_0	Initial contact length as illustrated in Fig. 1, m
L_c	Channel length as illustrated in Fig. 1, m
R	Cell radius, m
k	Bulk shear rate of channel flow, 1/s
$\boldsymbol{x}$	Vector of position at Eulerian grid
$\boldsymbol{u}$	Vector of velocity at Eulerian grid
t	Time, s
p	Pressure, Pa
$\boldsymbol{f_e}$	Vector of elastic force on cell membrane
$\boldsymbol{f_a}$	Vector of adhesion force on cell membrane
$\boldsymbol{x}'$	Vector of position at Lagrangian grid
h_e	Eulerian grid size, m
I	Indicator function in Eq. (9)
E	Elastic modulus of cell membrane, Pa
h	Thickness of cell membrane, m
l_{b0}, l_b	Length of unstressed and stressed adhesion bond, m
l_{mv0}, l_{mv}	Length of unstressed and stressed microvillus, m
k_b, k_{mv}	Spring constant of adhesion bond and microvillus, N/m
k_{ts}	Transition spring constant of adhesion bond
N_b, N_r, N_l	Density of adhesion bond, receptor and ligand
k_f, k_r	Forward and reverse reaction rate coefficients of adhesion bond
k_{bo}	Boltzmann constant
T	Absolute temperature
n_b	Number of adhesion bond
G	dimensionless stiffness of cell membrane, $G=\mu_0 kR/Eh$
D, θ	Deformation index and inclination angle as illustrated in Fig. 4a
D_c, θ_c	Deformation index and inclination angle as illustrated in Fig. 1c
t_c	Cell contact time, s

Greek letters

ρ_0, ρ_1, ρ_2	Density of surrounding fluid, cytoplasma and nucleus, kg/m^3
μ_0, μ_1, μ_2	Viscosity of surrounding fluid, cytoplasma and nucleus, $Pa \cdot s$
ε_1, ε_2	Principal stretch ratios of cell membrane
τ_w	Wall shear stress, Pa

Acknowledgment

This work was supported by the Specialized Research Fund for the Doctoral Program of Higher Education of China (20110201110029). This research was partially supported by the Foundation for Innovative Research Groups of the National Natural Science Foundation of China (Grant no. 50821064); the Major International (Regional) Joint Research Program of China (11120101002); Key (Key grant) Project of Chinese Ministry of Education (313045); the International Science & Technology Cooperation Program of China (2013DFG02930); National Natural Science Foundation of China (10825210, 31050110125); and the National 111 Project of China (B06024).

References

Bagchi, P., 2007. Mesoscale simulation of blood flow in small vessels. Biophys. J. 92, 1858–1877.

Bagchi, P., Johnson, P.C, Popel, A.S., 2005. Computational fluid dynamic simulation of aggregation of deformable cells in a shear flow. J. Biomech. Eng.-Trans. Asme 127, 1070–1080.

Bai, B.F., Luo, Z.Y., Lu, T.J., et al., 2013a. Numerical simulation of cell adhesion and detachment in microfluidics. J. Mech. Med. Biol. 13, 1350002.

Bai, B.F., Luo, Z.Y., Wang, S.Q., et al., 2013b. Inertia effect on deformation of viscoelastic capsules in microscale flows. Microfluidics Nanofluidics 14 817–829.

Bell, G.I., 1978. Models for specific adhesion of cells to cells. Science 200, 618–627.

Breyiannis, G, Pozrikidis, C., 2000. Simple shear flow of suspensions of elastic capsules. Theor. Comput. Fluid Dyn. 13, 327–347.

Bruehl, R.E., Springer, T.A, Bainton, D.F., 1996. Quantitation of l-selectin distribution on human leukocyte microvilli by immunogold labeling and electron microscopy. J. Histochem. Cytochem. 44, 835–844.

Cantat, I, Misbah, C., 1999. Lift force and dynamical unbinding of adhering vesicles under shear flow. Phys. Rev. Lett 83, 880–883.

Caputo, K.E., Lee, D., King, M.R., et al., 2007. Adhesive dynamics simulations of the shear threshold effect for leukocytes. Biophys. J. 92, 787–797.

Chang, K.C., Tees, D.F.J, Hammer, D.A., 2000. The state diagram for cell adhesion under flow: Leukocyte rolling and firm adhesion. Proc. Natl. Acad. Sci. USA 97, 11262–11267.

Cheng, X.H., Gupta, A., Chen, C.C., et al., 2009. Enhancing the performance of a point-of-care cd4+t-cell counting microchip through monocyte depletion for hiv/aids diagnostics. Lab Chip 9, 1357–1364.

Cheng, X.H., Irimia, D., Dixon, M., et al., 2007. A microfluidic device for practical label-free cd4+t cell counting of hiv-infected subjects. Lab Chip 7, 170–178.

Chesla, S.E., Selvaraj, P, Zhu, C., 1998. Measuring two-dimensional receptor-ligand binding kinetics by micropipette. Biophys. J. 75, 1553–1572.

Cheung, L.S.L., Zheng, X.G., Stopa, A., et al., 2009. Detachment of captured cancer cells under flow acceleration in a bio-functionalized microchannel. Lab Chip 9, 1721–1731.

Couzon, C., Duperray, A, Verdier, C., 2009. Critical stresses for cancer cell detachment in microchannels. Eur. Biophys. J. Biophys. Lett. 38, 1035–1047.

Decave, E., Garrivier, D., Brechet, Y., et al., 2002. Shear flow-induced detachment kinetics of dictyostelium discoideum cells from solid substrate. Biophys. J. 82, 2383–2395.

Dembo, M., Torney, D.C., Saxman, K., et al., 1988. The reaction-limited kinetics of membrane-to-surface adhesion and detachment. Proc. R. Soc. B-Biol. Sci. 234, 55–83.

Di Carlo, D., Irimia, D., Tompkins, R.G., et al., 2007. Continuous inertial focusing, ordering, and separation of particles in microchannels. Proc. Natl. Acad. Sci. U S A 104, 18892–18897.

Dong, C., Cao, J., Struble, E.J., et al., 1999. Mechanics of leukocyte deformation and adhesion to endothelium in shear flow. Ann. Biomed. Eng. 27, 298–312.

Eggleton, C.D, Popel, A.S., 1998. Large deformation of red blood cell ghosts in a simple shear flow. Phys. Fluids 10, 1834–1845.

Fischer, T.M., Stohrliesen, M, Schmidschonbein, H., 1978. Red-cell as a fluid droplet —tank tread-like motion of human erythrocyte-membrane in shear-flow. Science 202, 894–896.

Fritz, J., Katopodis, A.G., Kolbinger, F., et al., 1998. Force-mediated kinetics of single p-selectin ligand complexes observed by atomic force microscopy. Proc. Natl. Acad. Sci. U S A 95, 12283–12288.

Geissmann, F., Jung, S, Littman, D.R., 2003. Blood monocytes consist of two principal subsets with distinct migratory properties. Immunity 19, 71–82.

Huh, D., Gu, W., Kamotani, Y., et al., 2005. Microfluidics for flow cytometric analysis of cells and particles. Physiol. Meas. 26, R73–R98.

Hur, S.C., Henderson-MacLennan, N.K., McCabe, E.R.B., et al., 2011. Deformability-based cell classification and enrichment using inertial microfluidics. Lab Chip 11, 912–920.

Jadhav, S., Eggleton, C.D, Konstantopoulos, K., 2005. A 3-d computational model predicts that cell deformation affects selectin-mediated leukocyte rolling. Biophys. J. 88, 96–104.

Jin, Q., Verdier, C., Singh, P., et al., 2007. Migration and deformation of leukocytes in pressure driven flows. Mech. Res. Comm. 34, 411–422.

Kan, H.C., Udaykumar, H.S., Shyy, W., et al., 1999. Numerical analysis of the deformation of an adherent drop under shear flow. J. Biomech. Eng.-Trans. Asme 121, 160–169.

Khismatullin, D.B, Truskey, G.A., 2004. A 3d numerical study of the effect of channel height on leukocyte deformation and adhesion in parallel-plate flow chambers. Microvasc. Res. 68, 188–202.

Khismatullin, D.B, Truskey, G.A., 2005. Three-dimensional numerical simulation of receptor-mediated leukocyte adhesion to surfaces: Effects of cell deformability and viscoelasticity. Phys. Fluids, 17.

King, M.R, Hammer, D.A., 2001a. Multiparticle adhesive dynamics. Interactions between stably rolling cells. Biophys. J. 81, 799–813.

King, M.R, Hammer, D.A., 2001b. Multiparticle adhesive dynamics: hydrodynamic recruitment of rolling leukocytes. Proc. Natl. Acad. Sci. U S A 98, 14919–14924.

King, M.R., Heinrich, V., Evans, E., et al., 2005. Nano-to-micro scale dynamics of p-selectin detachment from leukocyte interfaces. III. Numerical simulation of tethering under flow. Biophys. J. 88, 1676–1683.

Liu, X.H, Wang, X., 2004. The deformation of an adherent leukocyte under steady shear flow: a numerical study. J. Biomech. 37, 1079–1085.

Luo, Z.Y., Xu, F., Lu, T.J., et al., 2011a. Direct numerical simulation of detachment of single captured leukocyte under different flow conditions. J. Mech. Med. Biol. 11, 273–284.

Luo, Z.Y., Xu, F., Lu, T.J., et al., 2011b. Direct numerical simulation of single leukocyte deformation in microchannel flow for disease diagnosis. J. Med. Syst. 35, 869–876.

Murthy, S.K., Sin, A., Tompkins, R.G., et al., 2004. Effect of flow and surface conditions on human lymphocyte isolation using microfluidic chambers. Langmuir 20, 11649–11655.

N'Dri, N.A., Shyy, W, Tran-Soy-Tay, R., 2003. Computational modeling of cell adhesion and movement using a continuum-kinetics approach. Biophys. J. 85, 2273–2286.

Nagrath, S., Sequist, L.V., Maheswaran, S., et al., 2007. Isolation of rare circulating tumour cells in cancer patients by microchip technology. Nature 450 1235-U1210.

Pappu, V, Bagchi, P., 2008. 3d computational modeling and simulation of leukocyte rolling adhesion and deformation. Comput. Biol. Med. 38, 738–753.

Pappu, V., Doddi, S.K, Bagchi, P., 2008. A computational study of leukocyte adhesion and its effect on flow pattern in microvessels. J. Theor. Biol. 254, 483–498.

Park, E.Y.H., Smith, M.J., Stropp, E.S., et al., 2002. Comparison of psgl-1 microbead and neutrophil rolling: Microvillus elongation stabilizes p-selectin bond clusters. Biophys. J. 82, 1835–1847.

Pawar, P., Jadhav, S., Eggleton, C.D., et al., 2008. Roles of cell and microvillus deformation and receptor-ligand binding kinetics in cell rolling. Am. J. Physiol.-Heart .Circ. Physiol. 295, H1439–H1450.

Phillips, A.N., Lee, C.A., Elford, J., et al., 1991. Serial lymphocyte-cd4 counts and development of aids. Lancet 337, 389–392.

Plouffe, B.D., Radisic, M, Murthy, S.K., 2008. Microfluidic depletion of endothelial cells, smooth muscle cells, and fibroblasts from heterogeneous suspensions. Lab Chip 8, 462–472.

Ramanujan, S, Pozrikidis, C., 1998. Deformation of liquid capsules enclosed by elastic membranes in simple shear flow: Large deformations and the effect of fluid viscosities. J. Fluid Mech. 361, 117–143.

Schmidschonbein, G.W., Shih, Y.Y, Chien, S., 1980. Morphometry of human-leukocytes. Blood 56, 866–875.

Shao, J.Y., Ting-Beall, H.P, Hochmuth, R.M., 1998. Static and dynamic lengths of neutrophil microvilli. Proc. Natl. Acad. Sci. U S A 95, 6797–6802.

Sin, A., Murthy, S.K., Revzin, A., et al., 2005. Enrichment using antibody-coated microfluidic chambers in shear flow: Model mixtures of human lymphocytes. Biotechnol. Bioeng. 91, 816–826.

Smerage, J.B, Hayes, D.F., 2006. The measurement and therapeutic implications of circulating tumour cells in breast cancer. Br. J. Cancer 94, 8–12.

Stott, S.L., Hsu, C.H., Tsukrov, D.I., et al., 2010a. Isolation of circulating tumor cells using a microvortex-generating herringbone-chip. Proc. Natl. Acad. Sci. U S A 107, 18392–18397.

Stott, S.L., Lee, R.J., Nagrath, S., et al., 2010b. Isolation and characterization of circulating tumor cells from patients with localized and metastatic prostate cancer. Sci. Trans. Med., 2.

Sui, Y., Chew, Y.T., Roy, P., et al., 2009. Inertia effect on the transient deformation of elastic capsules in simple shear flow. Comput. Fluids 38, 49–59.

Tryggvason, G., Bunner, B., Esmaeeli, A., et al., 2001. A front-tracking method for the computations of multiphase flow. J. Comput. Phys. 169, 708–759.

Tsai, M.A., Frank, R.S, Waugh, R.E., 1993. Passive mechanical-behavior of human neutrophils—power-law fluid. Biophys. J. 65, 2078–2088.

Unverdi, S.O, Tryggvason, G., 1992. A front-tracking method for viscous, incompressible, multi-fluid flows. J. Comput. Phys. 100, 25–37.

Verdier, C., Couzon, C., Duperray, A., et al., 2009. Modeling cell interactions under flow. J. Math. Biol. 58, 235–259.

Vonandrian, U.H., Hasslen, S.R., Nelson, R.D., et al., 1995. A central role for microvillous receptor presentation in leukocyte adhesion under flow. Cell 82, 989–999.

Zhang, X., Jones, P, Haswell, S.J., 2008. Attachment and detachment of living cells on modified microchannel surfaces in a microfluidic-based lab-on-a-chip system. Chem. Eng. J. 135, S82–S88.